CrystEngComm

Accepted Manuscript

CrystEngComm

Dynamic Article Links ►

Cite this: DOI: 10.1039/c0xx00000x

www.rsc.org/CrystEngComm

ARTICLE

Syntheses, Structures, and Magnetic Properties of Five Coordination Polymers Constructed From Biphenyl-3,4',5-Tricarboxylic Acid And (Bis)imidazole Linkers

Xiutang Zhang,[*a,b] Liming Fan,[a,b] Wei Zhang,[a] Weiliu Fan,[b] Liming Sun,[b] Xian Zhao[*b]

Received (in XXX, XXX) Xth XXXXXXXXX 2014, Accepted Xth XXXXXXXXX 2014
DOI: 10.1039/c0xx00000x

ABSTRACT: Five coordination polymers (CPs), namely, $\{[Ni_{1.5}(BPT)(1,4\text{-bib})_2(H_2O)]\cdot(1,4\text{-bib})_{0.5}\cdot 2H_2O\}_n$ (**1**), $\{[Co_2(BPT)(1,3\text{-bimb})(\mu_3\text{-}OH)]\cdot H_2O\}_n$ (**2**), $\{[Zn(HBPT)(1,3\text{-bimb})]\cdot H_2O\}_n$ (**3**), $\{[Co_2(BPT)(H_2BPT)(4,4'\text{-bibp})_2]\cdot 2H_2O\}_n$ (**4**), and $[Mn_{2.5}(BPT)(4,4'\text{-bibp})_{2.5}(SO_4)(H_2O)]_n$ (**5**) (H_3BPT = biphenyl-3,4',5-tricarboxylic acid, 1,4-bib = 1,4-bis(1H-imidazol-1-yl)benzene, 1,3-bimb = 1,3-bis(imidazol-1-ylmethyl)benzene, 4,4'-bibp = 4,4'-bis(imidazol-1-yl)biphenyl), were synthesized under hydrothermal conditions. Their structures have been determined by single-crystal X-ray diffraction analyses and further characterized by elemental analyses, IR spectra, powder X-ray diffraction (PXRD), and thermogravimetric (TG) analyses. Complex **1** exhibits an unprecedented 2D+2D→3D parallel entangled networks consisting of trilayer (3,4,6)-connected $(4^4.5^4.6^6.8)(5.6^4.8)_2(5^2.6^2)$ sheets. Complex **2** dispalys a 3D (3,10)-connected **3,10T9** net based on tetranuclear $\{Co_4(\mu_3\text{-}OH)_2\}$ clusters with the Schläfli symbol of $(4^{18}.6^{24}.8^3)(4^3)_2$. Complex **3** shows an interesting 1D tube-like chain including $Zn_2(1,3\text{-bimb})_2$ loops. Complex **4** affords 2D $(4^4.6^2)$-**sql** net constructed from $\{Co_2\}$ dinuclear units. Complex **5** dispalys a 3D 6-connected $(4^{12}.6^3)$-**pcu** net consisting of α-po primitive based on $\{Mn_5(SO_4)_2\}$ cluster. Moreover, magenetic studies indicate complexes **2**, **4** and **5** show antiferromagnetic properties.

Introduction

Recent research into coordination polymers (CPs) is attractive in the field of material science, due to their fascinating structures, new topological prototypes as well as the tremendous potential applications as functional materials in gas storage and separations,[1] ion exchange,[2] luminescence,[3] magnetism,[4] pohtocatalytic,[5] and heterogeneous catalysis.[6] Up to now, much efforts have been devoted and a large number of CPs with various architectures and excellent properties have been obtained through the self-assembly of selected or designed various organic ligands and metal ions or metal-oxide building units.

However, the controllable synthesis of prospective networks is still a far-reaching challenge, due to that such materials are always dependent on many uncertain factors, such as the coordination geometry preferred by the metal,[7] solvent system,[8] template,[9] pH value,[10] counteranion,[11] and the chemical structure of the selected ligands as well.[12] Among these factors, the rational selection of the characteristic ligand were proved to be one efficient route for the construction of versatile CPs. Generally, the length, rigidly, coordination modes, and functional groups or substituent of polycarboxylate ligands have consequential effect on the final structures of CPs.[13] Moreover, recent study on coordination assemblies using (bis)imidazole linkers as ancillary ligands states a reliable strategy for obtaining new topological prototypes of coordination nets.[14] The ancillary ligands have a great effect on the coordination modes of the host polycarboxylate aromatic acid and the final packing structures. With the length of the ancillary ligands increasing, the longer separation of neighboring central ions makes the host aromatic polycarboxylate ligand adopt more "open" coordination modes, and the overall structure a higher degree of interpenetration. The more flexibility of ancillary ligands could make the final structure more twisted and complicated.[15] Thus, CPs can be assembled from predetermined organic building blocks through judicious selection of ligands and careful control of reaction conditions. To the best of our knowledge, CPs based on biphenyl-3,4',5-tricarboxylic acid (H_3BPT) in the presence of (bis)imidazole linkers have never been documented to date.

Thus, these considerations inspired us to explore new coordination frameworks with biphenyl-3,4',5-tricarboxylic acid (H_3BPT) and bis(imidazole) bridging linkers (1,4-bib, 1,3-bimb, and 4,4'-bibp, Scheme 1). Herein, we reported the synthese and structural characterizations of five new coordination polymers, $\{[Ni_{1.5}(BPT)(1,4\text{-bib})_2(H_2O)]\cdot(1,4\text{-bib})_{0.5}\cdot 2H_2O\}_n$ (**1**), $\{[Co_2(BPT)(1,3\text{-bimb})(\mu_3\text{-}OH)]\cdot H_2O\}_n$ (**2**), $\{[Zn(HBPT)(1,3\text{-bimb})]\cdot H_2O\}_n$ (**3**), $\{[Co_2(BPT)(H_2BPT)(4,4'\text{-bibp})_2]\cdot 2H_2O\}_n$ (**4**),

[a] *Advanced Material Institute of Research, College of Chemistry and Chemical Engineering, Qilu Normal University, Jinan, 250013, China. E-mail: xiutangzhang@163.com.*
[b] *State Key Laboratory of Crystal Materials, Shandong University , Jinan 250100, China. E-mail: zhaoxian@icm.sdu.edu.cn.*

†Electronic Supplementary Information (ESI) available: Additional Figures, IR spectrum, Powder XRD patterns and X-ray crystallographic data, CCDC 977304-977308 for **1**-**5**. See DOI: 10.1039/c0xx00000x.

and $[Mn_{2.5}(BPT)(4,4'\text{-bibp})_{2.5}(SO_4)(H_2O)]_n$ (**5**), which exhibit a systematic variation of architectures from 1D ladder chain to 3D framework (Scheme 2) by the employment of H_3BPT and three bis(imidazole) bridging linkers (1,4-bib, 1,3-bimb, and 4,4'-bibp). Magnetic studies indicate that complexes of **2**, **4**, and **5** show antiferromagnetic behaviors.

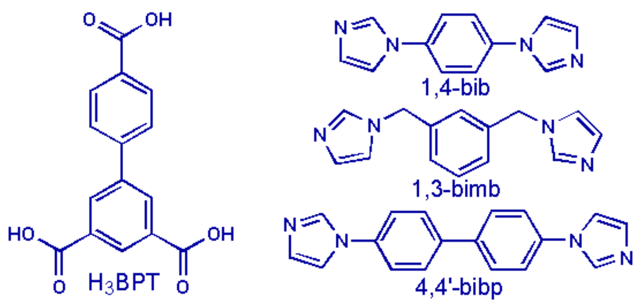

Scheme 1. Structures of H_3BPT and three bis(imdazole) bridging ligands.

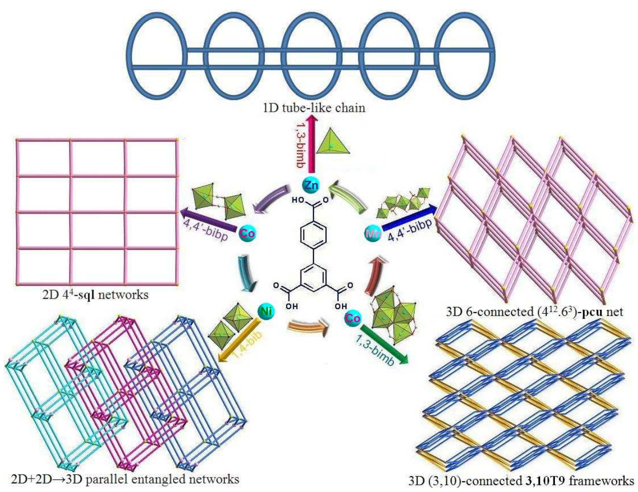

Scheme 2. Various structures of complexes **1–5**.

Experimental Section

Materials and Physical Measurements. All chemicals were purchased from Jinan Henghua Sci. & Tec. Co. Ltd. without further purification**.** IR spectra were measured on a Nicolet 740 FTIR Spectrometer at the range of 400-4000 cm^{-1}. Elemental analyses were carried out on a CE instruments EA 1110 elemental analyzer. X-ray powder diffractions were measured on a Panalytical X-Pert pro diffractometer with Cu-Kα radiation. Thermogravimetric analyses (TGA) were performed under air condition from room temperature to 800 °C with a heating rate of 10 °C min^{-1} on Perkin-Elmer TGA-7 thermogravimetric analyzer. The magnetic measurements were made with Quantum Design SQUID MPMS XL-7 instruments.

Synthesis of $\{[Ni_{1.5}(BPT)(1,4\text{-bib})_2(H_2O)]\cdot(1,4\text{-bib})_{0.5}\cdot 2H_2O\}_n$ (1). A mixture of H_3BPT (0.15 mmol, 0.043 g), 1,4-bib (0.20 mmol, 0.042 g), $NiSO_4\cdot 6H_2O$ (0.20 mmol, 0.053 g), NaOH (0.30 mmol, 0.012 g), and 12 mL H_2O was placed in a 25 mL Teflon-lined stainless steel vessel, heated to 170 °C for 3 days, followed by slow cooling (a descent rate of 10 °C/h) to room temperature. The green block crystals of **1** were obtained. Yield of 53% (based on Ni). Anal. (%) calcd. for $C_{90}H_{76}N_{20}Ni_3O_{18}$ (1901.84): C, 56.84; H, 4.03; N, 14.73. Found: C, 56.93; H, 3.76; N, 14.15. IR (KBr pellet, cm^{-1}): 3405 (m), 1603 (m), 1517 (s), 1387 (s), 1319 (m), 1074 (m), 831 (m), 713(w).

Synthesis of $\{[Co_2(BPT)(1,3\text{-bimb})(\mu_3\text{-OH})]\cdot H_2O\}_n$ (2). A mixture of H_3BPT (0.15 mmol, 0.043 g), 1,3-bimb (0.20 mmol, 0.048 g), $Co(NO_3)\cdot 6H_2O$ (0.20 mmol, 0.058 g), NaOH (0.30 mmol, 0.012 g), and 12 mL H_2O was placed in a 25 mL Teflon-lined stainless steel vessel, heated to 170 °C for 3 days, followed by slow cooling (a descent rate of 10 °C/h) to room temperature. The Red block crystals of **2** were obtained. Yield of 47% (based on Co). Anal. (%) calcd. for $C_{29}H_{24}Co_2N_4O_8$ (674.38): C, 51.65; H, 3.59; N, 8.31. Found: C, 51.43; H, 3.43; N, 8.77. IR (KBr pellet, cm^{-1}): 3467 (m), 1619 (s), 1596 (s), 1567 (s), 1398 (s), 1274 (w), 1087 (w), 978 (w), 836 (w), 722 (m).

Table 1 Crystal data for **1 – 5**

Compound	1	2	3	4	5
Empirical formula	$C_{90}H_{76}N_{20}Ni_3O_{18}$	$C_{29}H_{24}Co_2N_4O_8$	$C_{29}H_{24}N_4O_7Zn$	$C_{67}H_{49}Co_2N_8O_{14}$	$C_{120}H_{88}Mn_5N_{20}O_{22}S_2$
Formula weight	1901.84	674.38	605.89	1308.00	2500.92
Crystal system	Triclinic	Monoclinic	Triclinic	Monoclinic	Triclinic
Space group	*P*-1	*P*2(1)/*n*	*P*-1	*P*2(1)	*P*-1
a (Å)	13.4907(14)	12.337(2)	8.9151(10)	11.7332(4)	12.150(3)
b (Å)	13.5050(14)	11.051(2)	12.3303(13)	15.2259(6)	13.422(3)
c (Å)	13.7924(14)	21.819(4)	13.3052(14)	16.1433(6)	17.825(4)
α (°)	102.084(2)	90	108.564(2)	90	77.205(4)
β (°)	97.561(2)	100.761(4)	107.760(2)	102.4970(10)	70.985(4)
γ (°)	116.001(2)	90	99.002(2)	90	83.344(4)
$V(Å^3)$	2136.0(4)	2922.3(9)	1267.3(2)	2815.65(18)	2676.8(10)
Z	1	4	2	2	1
D_{calcd} (g/cm^3)	1.479	1.533	1.588	1.543	1.551
μ(mm^{-1})	0.738	1.192	1.028	0.670	0.699
R_{int}	0.0168	0.0673	0.0420	0.0250	0.0342
Final *R* indices[$I > 2\sigma(I)$]	$R_1 = 0.0464$ $wR_2 = 0.1283$	$R_1 = 0.0470$ $wR_2 = 0.0971$	$R_1 = 0.0450$ $wR_2 = 0.1228$	$R_1 = 0.0452$ $wR_2 = 0.1183$	$R_1 = 0.0690$ $wR_2 = 0.1102$
R indices (all data)	$R_1 = 0.0582$ $wR_2 = 0.1381$	$R_1 = 0.0811$ $wR_2 = 0.1138$	$R_1 = 0.0574$ $wR_2 = 0.1378$	$R_1 = 0.0519$ $wR_2 = 0.1237$	$R_1 = 0.1185$ $wR_2 = 0.1581$
Gof	1.003	1.001	0.997	1.002	1.000

$R_1 = \Sigma||F_o|-|F_c||/\Sigma|F_o|$, $wR_2 = [\Sigma w(F_o^2-F_c^2)^2]/\Sigma w(F_o^2)^2]^{1/2}$

Synthesis of $\{[Zn(HBPT)(1,3\text{-bmib})]\cdot H_2O\}_n$ (3). A mixture of H_3BPT (0.20 mmol, 0.057 g), 1,3-bmib (0.20 mmol, 0.048 g), $ZnSO_4\cdot 7H_2O$ (0.30 mmol, 0.086 g), $(NH_4)_6Mo_7O_{24}\cdot 4H_2O$ (0.81 mmol, 0.100 g), NaOH (0.20 mmol, 0.008 g), and 15 mL H_2O was placed in a 25 mL Teflon-lined stainless steel vessel, heated to 170 °C for 3 days, followed by slow cooling (a descent rate of 10 °C/h) to room temperature. The colorless block crystals of **3** were obtained. Yield of 42% (based on Zn). Anal. (%) calcd. for $C_{29}H_{24}N_4O_7Zn$ (605.89): C, 57.48; H, 3.99; N, 9.25. Found: C, 57.89; H, 4.03; N, 9.38. IR (KBr pellet, cm^{-1}): 3469 (m), 1621 (s), 1536 (s), 1394 (s), 1284 (w), 1109 (m), 944 (w), 778 (w), 730 (m).

Synthesis of $\{[Co_2(BPT)(H_2BPT)(4,4'\text{-bibp})_2]\cdot 2H_2O\}_n$ (4). A mixture of H_3BPT (0.15 mmol, 0.043 g), 4,4'-bibp (0.40 mmol, 0.114 g), $Co(NO_3)\cdot 6H_2O$ (0.40 mmol, 0.116 g), NaOH (0.30 mmol, 0.012 g), and 12 mL H_2O was placed in a a 25 mL Teflon-lined stainless steel vessel, heated to 170 °C for 3 days, followed by slow cooling (a descent rate of 10 °C/h) to room temperature. The Red block crystals of **4** were obtained. Yield of 47% (based on Co). Anal. (%) calcd. for $C_{67}H_{49}Co_2N_8O_{14}$ (1308.00): C, 61.52; H, 3.78; N, 8.57. Found: C, 61.21; H, 3.71; N, 8.69. IR (KBr pellet, cm^{-1}): 3431 (m), 3128 (m), 1605 (m), 1509 (s), 1382 (s), 1301 (s), 1060 (m), 814 (m), 658 (w).

Synthesis of $[Mn_{2.5}(BPT)(4,4'\text{-bibp})_{2.5}(SO_4)(H_2O)]_n$ (5). The same synthetic procedure as for **4** was used except that $Co(NO_3)\cdot 6H_2O$ was replaced by $MnSO_4\cdot H_2O$, giving yellow block crystals. Yield of 43% (based on Mn). Anal. (%) calcd. for $C_{120}H_{88}Mn_5N_{20}O_{22}S_2$ (2500.92): C, 57.63; H, 3.55; N, 11.20. Found: C, 57.89; H, 3.72; N, 10.93. IR (KBr pellet, cm^{-1}): 3445 (m), 3123 (m), 1604 (s), 1509 (vs), 1291 (s), 1051 (s), 819 (s), 724 (w).

X-ray Crystallography. Intensity data collection was carried out on a Siemens SMART diffractometer equipped with a CCD detector using Mo-Kα monochromatized radiation (λ=0.71073Å) at 293(2) or 296(2) K. The absorption correction was based on multiple and symmetry-equivalent reflections in the data set using the SADABS program based on the method of Blessing. The structures were solved by direct methods and refined by full-matrix least-squares using the SHELXTL package.[16] All non-hydrogen atoms were refined anisotropically. Hydrogen atoms except those for water molecules were generated geometrically with fixed isotropic thermal parameters, and included in the structure factor calculations. The approximate positions of the water H atoms, obtained from a difference Fourier map, were restrained to ideal configuration of the water molecule and fixed in the final stages of refinement. Four carbon atoms from one phenyl ring of BPT^{3-} in compound **1** are disordered and refined with an occupancy ratio of 40:60. For **1** and **4**, there are some very large ADPs in the (Bis)imidazole linkers. Crystallographic data for compounds **1**–5 are given in Table 1. Selected bond lengths and angles are listed in Table S1. For complexes of **1**–**5**, further details on the crystal structure investigations can be obtained from the Cambridge Crystallographic Data Centre, CCDC, 12 Union Road, CAMBRIDGE CB2 1EZ, UK, [Telephone: +44-(0)1223-762-910, Fax: +44-(0)1223-336-033; Email: deposit@ccdc.cam.ac.uk, http://www.ccdc.cam.ac.uk/ deposit], on quoting the depository number CCDC-977304 for **1**, 977305 for **2**, 977306 for **3**, 977307 for **4**, 977308 for **5**. Topological analysis of the coordination networks of all the compounds was performed with the program package TOPOS.[17]

Result and Discussion

Synthesis and General Characterization. In the present study, complexes **1**-5 were prepared from the solvothermal reaction of the related first transitional metal salts and the H_3BPT in the presence of rigid or flexible (bis)imidazole bridging linkers (1,4-bib, 1,3-bimb, and 4,4'-bibp). All the complexes **1-5** are stable in the solid state upon extended exposure to air. They have poor solubility in water and common organic solvents, but can be slightly soluble in very high polarity solvents.

Powder X-ray diffraction (PXRD) has been used to check the phase purity of the bulk samples in the solid state. For complexes **1**−**5**, the measured PXRD patterns closely match the simulated patterns generated from the results of single crystal diffraction data, indicative of pure products (Fig. S1, see Supporting Information). The absorption bands in the range of 3400-3500 cm^{-1} for **1-5** can be attributed to the characteristic peaks of water O-H vibrations. The vibrations at ca. 1520 and 1610 cm^{-1} correspond to the asymmetric and symmetric stretching vibrations of the carboxylate groups, respectively (Fig. S2).

Structure descriptions of $\{[Ni_{1.5}(BPT)(1,4\text{-bib})_2(H_2O)]\cdot(1,4\text{-bib})_{0.5}\cdot 2H_2O\}_n$ (1). The single-crystal X-ray diffraction analysis reveals that complex **1** crystallizes in the triclinic system, *P*-1 space group. As shown in Fig. 1a, there are one and a half of Ni^{II} ions, one completely deprotonated BPT^{3-} ligand, two 1,4-bib ligands, one coordinated water molecule, and guest molecules including a half of 1,4-bib and two water molecules in the asymmetric unit. The Ni(1) cation is coordinated by four oxygen atoms from two BPT^{3-} ligands and one water molecule, and two nitrogen atoms from two individual 1,4-bib ligands, leaving a distorted octahedral geometry. Ni(2) is coordinated by two oxygen atoms from two BPT^{3-} ligands, and two nitrogen atoms from two 1,4-bib ligands. The bond lengths of Ni–O and Ni–N are in the range of 1.9968(18)–2.1957(17) Å and 2.053(2)–2.121(2) Å, respectively. The ligand of BPT^{3-} exhibits $(\kappa^1\text{-}\kappa^0)\text{-}(\kappa^1\text{-}\kappa^0)\text{-}(\kappa^1\text{-}\kappa^1)\text{-}\mu_3$ coordination mode (Mode I, Scheme 3) and connect three Ni^{II} ions to form a 1D $[Ni_3(BPT)_2]_n$ ladder chain (Fig. S3).

Ni(1) ions are linked by 1,4-bib ligands to form a 2D $[Ni(1,4\text{-bib})_2]_n$ net along *bc* plane (Fig. S4). Above and below $[Ni(1,4\text{-bib})_2]_n$ layer, another two layers are constructed from the mixed ligands of 1,4-bib and BPT^{3-}. These three coordination planes are further linked though the $(\kappa^1\text{-}\kappa^0)\text{-}\mu_1$ carboxyl groups, generated a 2D network containing the cavity of 13.505(0) × 13.792(4) × 18.380(9) $Å^3$ (Fig. 1b). The 2D networks are further connected with each other, finally resulting in a 2D+2D→3D parallel framework (Fig. 1c). It is noteworthy that the guest molecules (1,4-bib, H_2O) occupied the channels *via* hydrogen bonds, which may be one important factor to stabilize the whole framework. Besides, PLATON[18] calculated the void volume of **1** is 1.8% (38.2 out of the 2136.0 $Å^3$ unit cell volume).

The topology analysis shows that the overall framework of complex **1** can be rationalized to a trinodal (3,4,6)-connected net with the point symbol of $(4^4.5^4.6^6.8)(5.6^4.8)_2(5^2.6^2)$ by denoting

BPT^{3-}, Ni(1), and Ni(2) as 3-connected, 6-connected, and 4-connected nodes, respectively (Fig. 1d).

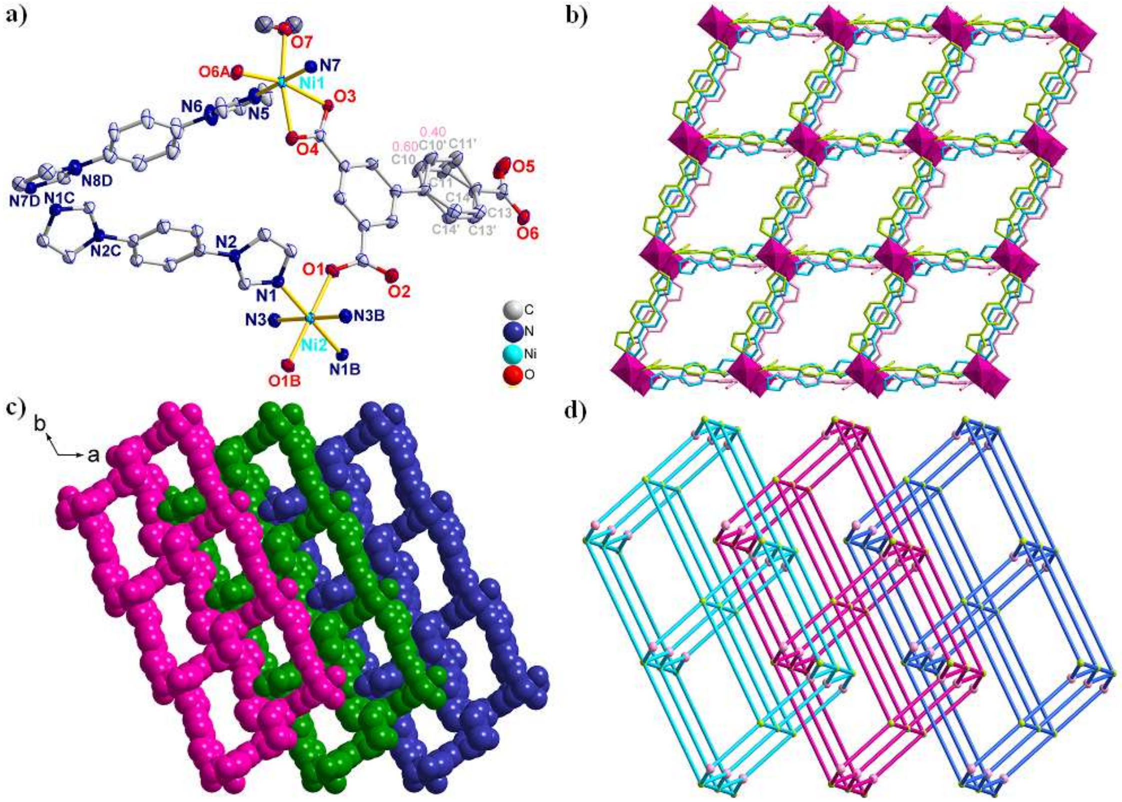

Figure 1. (a) ORTEP representation of **1** with 50% thermal ellipsoid probability. Guest molecules and hydrogen atoms are omitted for clarity. Symmetry codes: A: *x*, *y*, -1+*z*; B: 2-*x*, 1-*y*, 1-*z*; C: 2-*x*, 1-*y*, -*z*; D: *x*, 1+*y*, *z*. (b) The unprecedented $Ni_2(BPT)(1,4\text{-bib})_2$ trilayer. (c) The 2D+2D→3D parallel entangled networks view along *c* axis. (d) The 2D+2D→3D interpenetrated (3,4,6)-connected topology $(4^4.5^4.6^6.8)(5.6^4.8)_2(5^2.6^2)$ sheets in **1**.

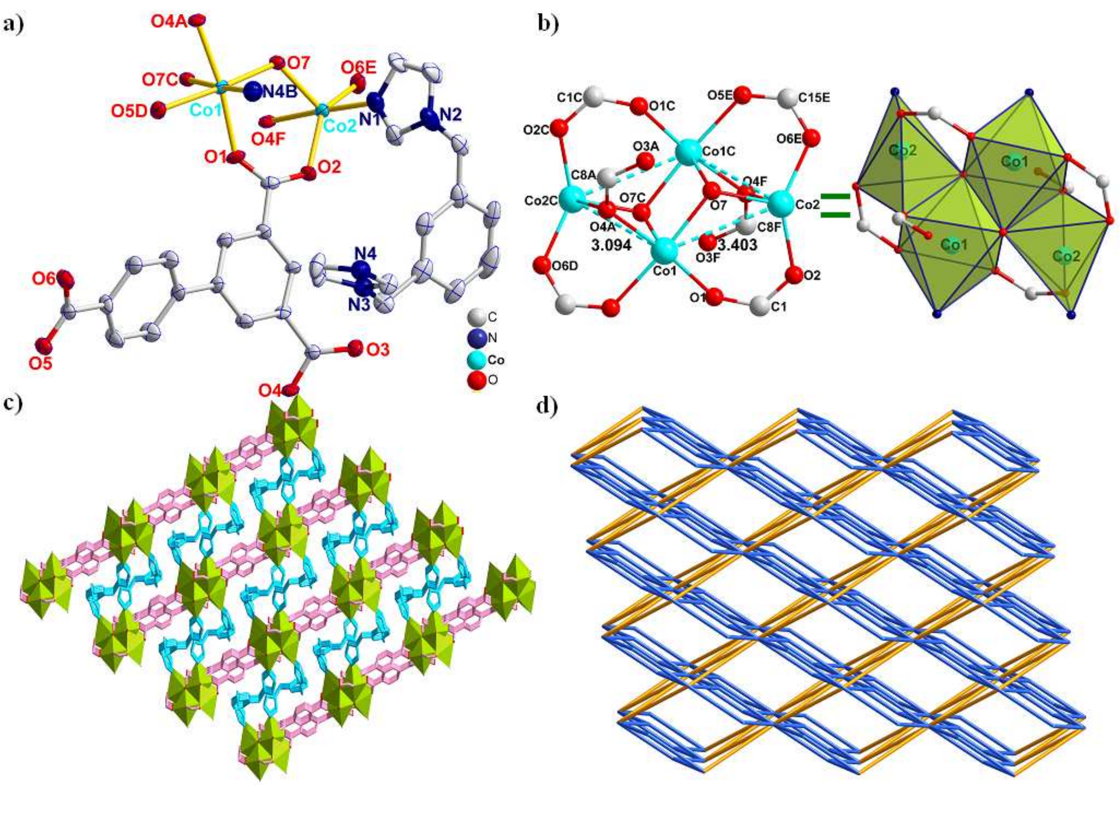

Figure 2. (a) ORTEP representation of **2** with 50% thermal ellipsoid probability. Hydrogen atoms are omitted for clarity. Symmetry codes: A: *x*, 1+*y*, *z*; B: 1.5-*x*, 0.5+*y*, 0.5-*z*; C: 2-*x*, 2-*y*, 1-*z*; D: 2.5-*x*, 0.5+*y*, 0.5-*z*; E: -0.5+*x*, 1.5-*y*, 0.5+*z*; F: 2-*x*, 1-*y*, 1-*z*. (b) The $Co_4(COO)_6(\mu_3\text{-}OH)_2$ SBUs in **2**. (c) A perspective view of the 3D frameworks view along *b* axis. (d) The 3D (3,10)-connected **3,10-T9** topology with the Schläfli symbol of $(4^{18}.6^{24}.8^3)_2$ in **2**.

Structure descriptions of $\{[Co_2(BPT)(1,3\text{-bimb})(\mu_3\text{-}OH)]\cdot H_2O\}_n$ (2). The application of 1,3-bimb during the syndesis of **2**, more flexible and longer than 1,4-bib applied in complex **1**, results in a 3D high connected framework consisting of the $[Co_4(\mu_3\text{-}OH)_2]^{6+}$ tetrameric SBUs in **2**. This proves that, with the length and flexibility of the ancillary ligands increasing, the longer separation of neighboring central ions makes the host aromatic polycarboxylate ligand adopt more "open" coordination modes, and the overall structure exhibits a higher degree of interpenetration. [15c]

Complex **2** crystallizes in the monoclinic system, $P2_1/n$ space group. The asymmetric unit of complex **2** consists of two Co^{II} ions, one BP T^{3-} ligand, one 1,3-bimb ligand, one μ_3-OH^- anion, and one lattice water molecule (Fig. 2a). Four Co^{II} ions are connected though μ_3-OH, giving a parallelogram $[Co_4(\mu_3\text{-}OH)_2]^{6+}$ tetrameric SBUs, with the Co···Co distances of 3.403 Å and 3.094 Å (Fig. 2b). Co(1) is located in a distorted octahedral $\{CoO_5N\}$ geometry, coordinated by the three carboxylate oxygen atoms from three BPT^{3-} ligands, two μ_3-OH oxygen atoms, and one nitrogen atom from a 1,4-bib ligand. Whereas, Co(2) is located in a distorted trigonal bipyramidal CoO_4N geometry, coordinated by four carboxylate oxygen atoms from three different BPT^{3-} ligands and one μ_3-OH, and one nitrogen atom from one 1.3-bimb ligand. The Co-O bond lengths are in the range of 1.968(3)–2.253(3) Å, and the Co-N bond distances are 2.057(4) and 2.114(3) Å, respectively.

The BPT^{3-} ligand exhibits an unreported $(\kappa^1\text{-}\kappa^1)\text{-}(\kappa^1\text{-}\kappa^1)\text{-}(\kappa^0\text{-}\kappa^2)\text{-}\mu_6$ coordination mode (Mode II) linking the $[Co_4(\mu_3\text{-}OH)_2]^{6+}$ tetrameric SBUs, finally resulting in a 2D $[Co_2(\mu_3\text{-}OH)(BTB)_3]_n$ bilayer (Fig. S5). The bilayers are further expanded by the 1,3-bimb ligands to form a 3D framework (Fig. 2c). The Co···Co distances separated by μ_6-BPT^{3-} are 14.632, 14.540 and 14.051 Å, respectively.

From the viewpoint of structural topology, the whole structure of complex **2** can be defined as a binodal (3,10)-connected **3,10-T9** topology with the short Schläfli symbol of $(4^{18}.6^{24}.8^3)_2$ by denoting the $[Co_4(\mu_3\text{-}OH)_2]^{6+}$ tetrameric SBUs to ten connected nodes and BPT^{3-} ligands to three-connected nodes, respectively (Fig. 2d).

Structure descriptions of $\{[Zn(HBPT)(1,3\text{-bmib})]\cdot H_2O\}_n$ (3). The single-crystal X-ray diffraction analysis reveals that complex **3** crystallizes in the triclinic system, *P*-1 space group. As shown in Fig. 3a, there are one one Zn^{II} ion, one partly deprotonated $HBTB^{2-}$ ligand, one 1,3-bmib ligand, and one lattice water molecule in the asymmetric unit. Zn(1) is tetra-coordinated, completed by two oxygen atoms from two different $HBPT^{2-}$ ligands [Zn(1)-O(1) = 1.963(3) and Zn(1)-O(5B) = 1.964(2) Å] and two nitrogen atoms from two individual 1,3-bmib ligands [Zn(1)-N(1) = 2.046(3) and Zn(1)-N(4A) = 2.048(3) Å], resulting in a distorted tetrahedral coordination geometry. The bond angles around Zn^{II} cation range from 94.28(12) to 123.15(12)°.

The H_3BPT ligands in complex **3** are partly deprotonated and exhibit $(\kappa^1\text{-}\kappa^0)\text{-}(\kappa^1\text{-}\kappa^0)\text{-}\mu_2$ coordination mode (Mode III). Each $HBPT^{2-}$ ligand connected two Zn^{II} ions to form a 1D straight $[Zn(HBPT)]_n$ chain. Neighbour two chains are linked *via* two bent 1,3-bimb ligands to form a 1D tube-like chain consisting of rhombus $[Zn_2(1,3\text{-bimb})_2]$ metallamacrocycles (Fig. 3b). The adjacent tube-like chains interacted with each other though O-H···π [O4-H4w···π = 3.794 (0) Å], leaving a supramolecular architecture (Fig. 3c).

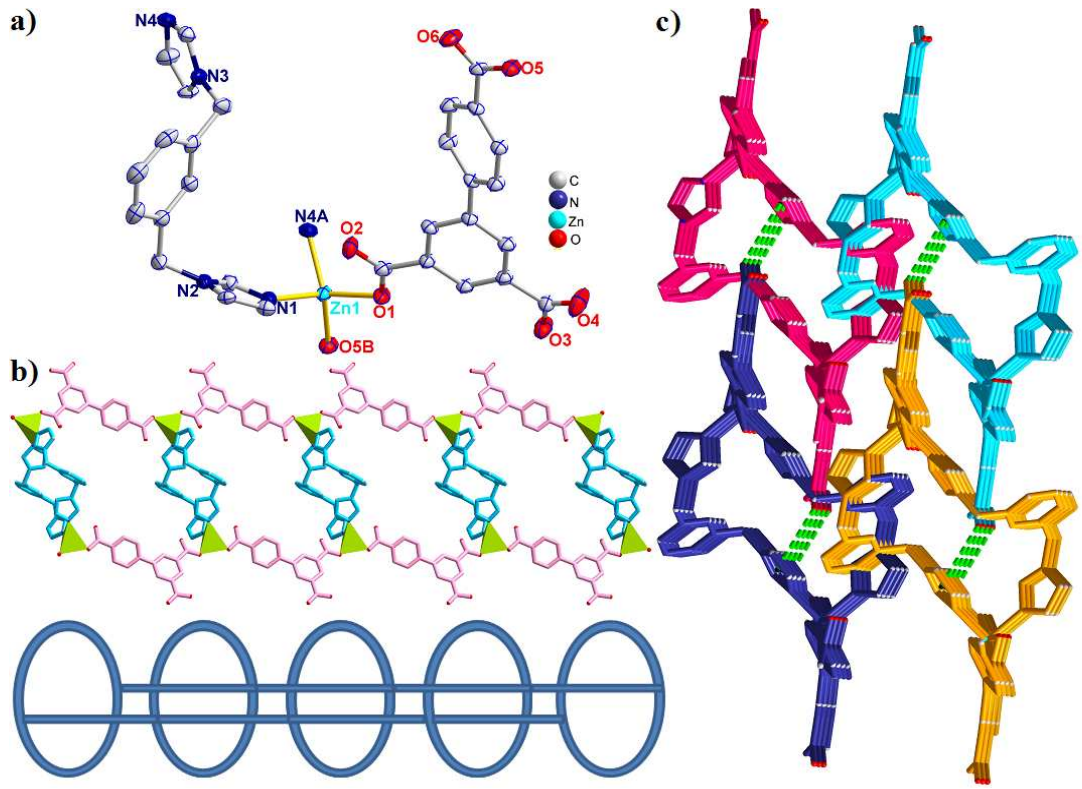

Figure 3. (a) ORTEP representation of **3** with 50% thermal ellipsoid probability. Hydrogen atoms are omitted for clarity. Symmetry codes: A: -*x*, 2-*y*, 2-*z*; B: 1+*x*, 1+*y*, *z*. (b) Schematic view of the 1D tube-like chain and topology. (c) The 3D supramolecular connected though O-H···π interactions.

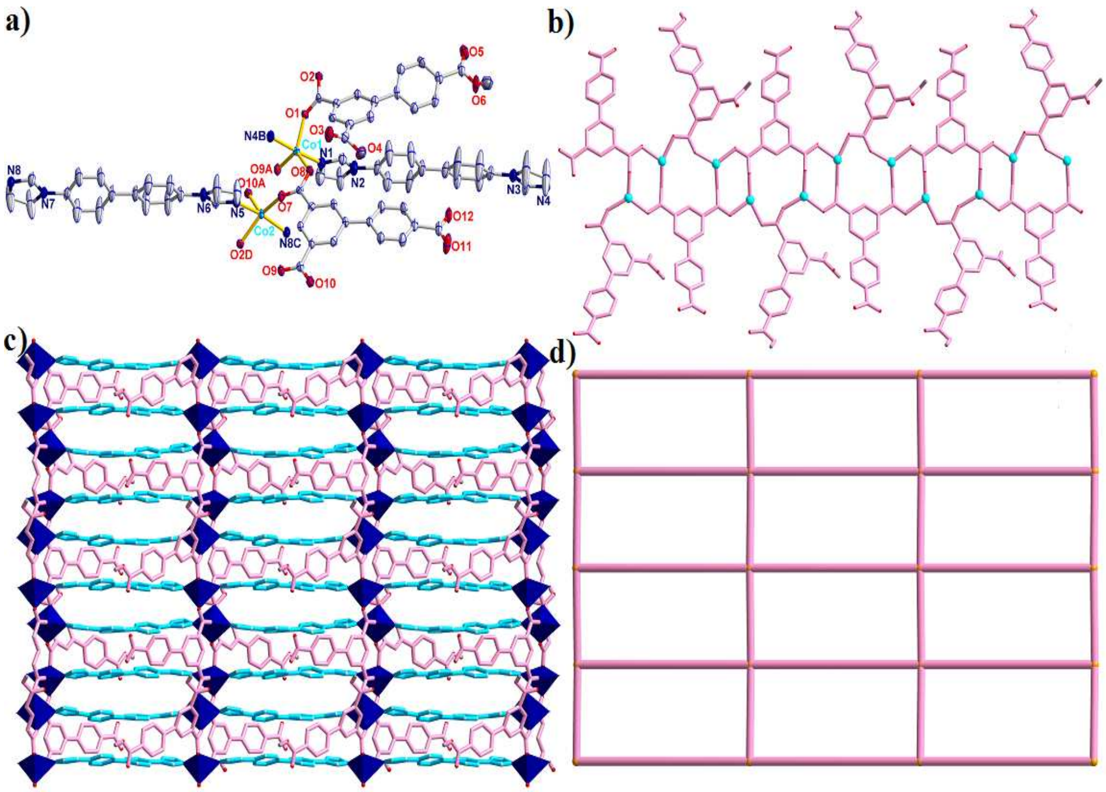

Figure 4. (a) ORTEP representation of **4** with 50% thermal ellipsoid probability. Hydrogen atoms are omitted for clarity. Symmetry codes: A: 2-*x*, -0.5+*y*, 2-*z*; B: 1+*x*, *y*, 1+*z*; C:-1+*x*, *y*, -1+*z*. (b) The 1D $[Co_2(BPT)(H_2BPT)]_n$ ladder chain. (c) The 2D networks constructed by the 1D chains sharing the $[Co_2(COO)_2]$ SBUs. (d) The $(4^4.6^2)$-**sql** topology of the 2D nets in **4**.

Structure descriptions of $\{[Co_2(BPT)(H_2BPT)(4,4'\text{-bibp})_2]\cdot 2H_2O\}_n$ (4). Structure analysis reveals that complex **4** crystallizes in the monoclinic system, $P2_1$ space group. As shown in Fig. 4a, the asymmetric unit consists of two Co^{II} ions, one BPT^{3-} ligand, one partly deprotonated H_2PBT^- ligand, two 4,4'-bibp ligands, and two lattice water molecules. Both Co(1) and Co(2) are penta-coordinated by three oxygen atoms from one BPT^{3-} and H_2BPT^- ligands, and two nitrogen atoms from two 4,4'-bibp ligands. The bond lengths of Co–O and Co-N are in the range of 1.990(2)-2.104(2) and 2.072(3)-2.123(3) Å, respectively.

BPT^{3-} ligand exhibits two kinds of novel coordination modes in the assembly of complex **4**: the partly deprotonated one owns $(\kappa^1\text{-}\kappa^1)\text{-}\mu_2$ coordination mode (Mode IV), and the completely deprotonated one displays $(\kappa^0\text{-}\kappa^0)\text{-}(\kappa^1\text{-}\kappa^1)\text{-}(\kappa^1\text{-}\kappa^1)\text{-}\mu_4$ coordination mode (Mode V). Co^{II} ions are coordinated by BPT^{3-} and $HBPT^{2-}$ in stagger, forming a $[Co_2(COO)_2]$ SBUs based 1D ladder chain with the Co···Co distances being 3.965, and 4.682 Å, respectively (Fig. 4b). Along the *c* axis, the 1D chains are linked by 4,4'-bibp ligands, resulting in a 2D network (Fig. 4c). Topology analysis reveal that the whole structure can be view as a $(4^4.6^2)$-**sql** net by denoting the $[Co_2(COO)_2]$ SBUs as 4-connected nodes (Fig. 4d).

Structure descriptions of $[Mn_{2.5}(BPT)(4,4'\text{-bibp})_{2.5}(SO_4)(H_2O)]_n$ (5). Similar reaction environment to 4, except for $MnSO_4\cdot H_2O$ replacing $Co(NO_3)\cdot 6H_2O$, results in one 3D 6-connected **pcu** framework. Structure analysis reveals that complex **5** crystallizes in the triclinic system, space group *P*-1. The asymmetric unit of **5** contains two and a half of Mn^{II} ion, one BPT^{3-} ligand, two and a half of 4,4'-bibp ligands, one SO_4^{2-} anion, and one coordinated water molecule, shown in Fig. 5a. Mn(1) is hexa-coordinated, completed by four oxygen atoms from two different BPT^{3-} ligands and two SO_4^{2-} anions, and two nitrogen atoms from two individual 4,4'-bibp ligands, leaving a distorted octahedral coordination geometry. Mn(2) is coordinated by two oxygen atoms from two BPT^{3-}ligands, one oxygen atom from SO_4^{2-} anion, one associated water molecule, and two nitrogen atoms from two 4,4'-bibp ligands. Mn(3) is coordinated by two oxygen atoms from two BPT^{3-} ligands, and another two oxygen atoms from one SO_4^{2-} anion, and two nitrogen atoms from two 4,4'-bibp ligands. The bond lengths of Mn–O and Mn–N are in the range of 2.120(2)–2.3326(19) and 2.220(3)–2.304(2) Å, respectively.

The BPT^{3-} ligand in complex **5** is completely deprotonated and exhibits $(\kappa^1\text{-}\kappa^0)\text{-}(\kappa^1\text{-}\kappa^1)\text{-}(\kappa^1\text{-}\kappa^1)\text{-}\mu_5$ coordination mode (Mode VI). Mn^{II} cations are bridged by $(\kappa^1\text{-}\kappa^1)\text{-}\mu_2$ carboxylate group and μ_3-SO_4^{2-} anion to generate a 2D network consisting of unprecedented pentanuclear $[Mn_5(COO)_6(SO_4)_2]$ SBUs with Mn···Mn distances being 4.053 Å (for Mn1-Mn3), 3.902 Å (for Mn2-Mn3), and 6.774 Å (for Mn1-Mn2), respectively (Fig. 5b, S6). The networks are further linked by two 4,4'-bibp ligands to result in a 3D framework (Fig. 5c).

From the viewpoint of structural topology, the whole 3D structure exhibits a 6-connected **pcu** net with α-po primitive cubic nets with the short point symbol of $(4^{12}.6^3)$ by denoting $[Mn_5(COO)_6(SO_4)_2]$ SBUs as 6-connected node (Fig. 5d).

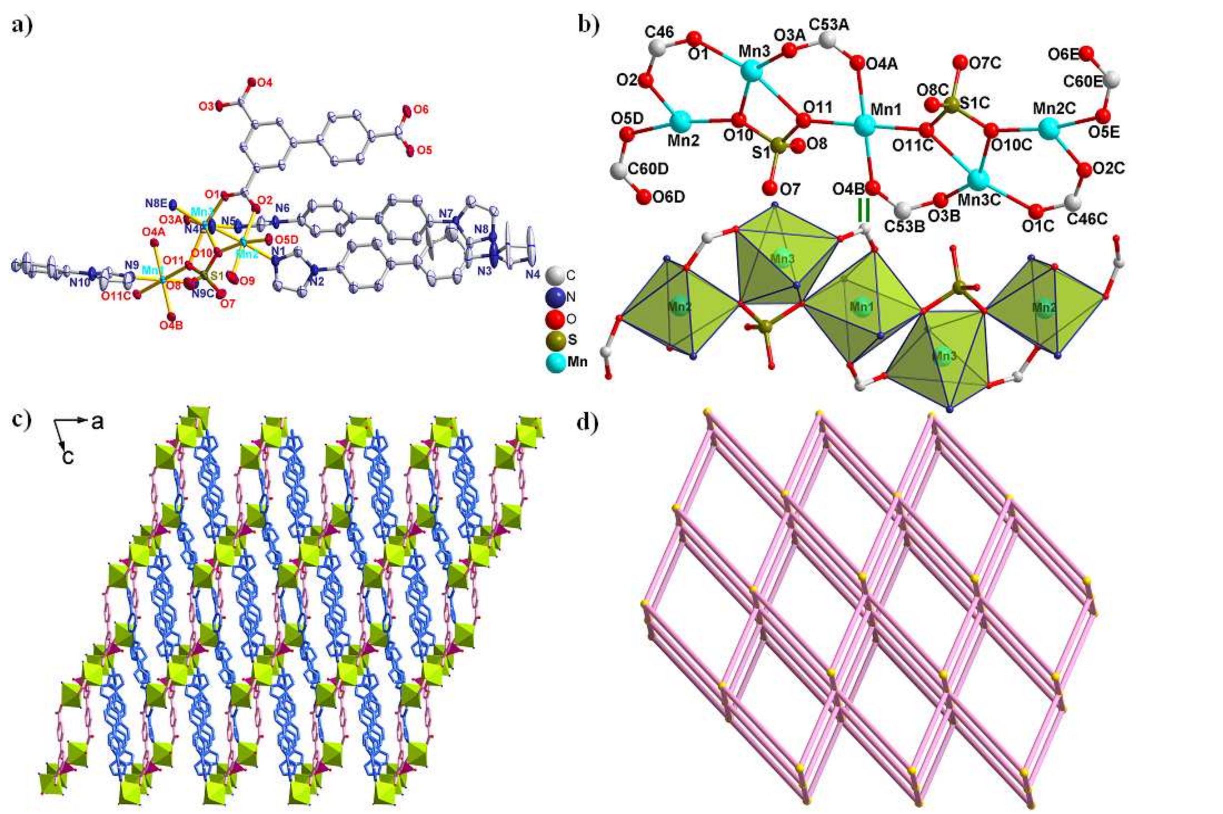

Figure 5. (a) ORTEP representation of **5** with 50% thermal ellipsoid probability. Hydrogen atoms are omitted for clarity. Symmetry codes: A: 1-*x*, 2-*y*, 1-*z*; B: *x*, -1+*y*, *z*; C: 1-*x*, 1-*y*, 1-*z*; D: -*x*, 2-*y*, 2-*z*; E: *x*, *y*, 1-*z*. (b) The $[Mn_5(COO)_6(SO_4)_2]$ SBUs in compound **5**. (c) A perspective view of 3D frameworks view along *b* axis. (d) The 3D 6-connected **pcu**-α-po topology with the Schläfli symbol of $(4^{12}.6^3)$ in **5**.

Table 2 The coordination types of H_3BPT ligand and the roles of ancillary ligands in complexes **1**–**5** and other ancillary ligands modified CPs.

Compound	Coord. Modes	Ancillary Ligands/Role	Dihedral Angles (°)	Structure and Topology
1	Mode I	1,4-bib/bridging+guest	20.27(1)	2D→3D $(4^4.5^4.6^6.8)(5.6^4.8)_2(5^2.6^2)$ net
2	Mode II	1,3-bimb/bridging	38.22(4)	3D (3,10)-connected $(4^{18}.6^{24}.8^3)(4^3)_2$ net
3	Mode III	1,3-bimb/bridging	37.99(3)	1D tube-like chain
4	Mode IV/V	4,4'-bibp/bridging	33.09(2)/16.20(8)	2D 4-connected $(4^4.6^2)$ net
5	Mode VI	4,4'-bibp/bridging	8.06(7)	3D 6-connected $(4^{12}.6^3)$ net
$[Cd_3(BPT)_2(phen)_3]$[19a]	Mode VII	phen/cheating	23.86(8)	1D→2D interdigitated structure
$[Mn_5(HBPT)_4(phen)_4]$[19b]	Mode VIII/IX	phen/cheating	28.69(1)/30.12(8)	2D 4-connected $(4^4.6^2)$ net
$[Cd_2(BPT)(phen)_2]$[19b]	Mode X	phen/cheating	37.06(3)	1D wave ladder chain
$[Cu_2(BPT)(phen)]$[19b]	Mode XI	phen/cheating	8.61(1)	2D 3-connected (4.8^2) net
$[Mn(HBPT)_4(4,4'\text{-bipy})_{0.5}]$[19c]	Mode XI	4,4'-bipy/bridging	34.05(0)	2D 4-connected $(4^4.6^2)$ net
$[Cd(HBPT)(4,4'\text{-bipy})_{0.5}]$[19b]	Mode XI	4,4'-bipy/bridging	34.95(1)	2D 4-connected $(4^4.6^2)$ net
$[Co(HBPT)_4(4,4'\text{-bipy})_{0.5}]$[19c]	Mode XII	4,4'-bipy/bridging	34.84(9)	2D 4-connected $(4^4.6^2)$ net

Notes: all the solvent molecules were omitted from the formulas. Abbreviation: phen = phenanthroline; 4,4'-bipy = 4,4'-bipyridine.

The diverse coordination modes of H_3BPT and the structural comparison. As shown in the Scheme 3 and Table 2, H_3BPT exhibits versatile coordination modes and results in different new topologies. In complex **1**, H_3BPT is completely deprotonated and connects nickel ions *via* $(\kappa^1\text{-}\kappa^1)\text{-}(\kappa^1\text{-}\kappa^0)\text{-}(\kappa^1\text{-}\kappa^0)\text{-}\mu_3$ coordination mode (Mode I), resulting in a ladder chain. The BPT^{3-} ligand in complex **2** exhibit $(\kappa^1\text{-}\kappa^1)\text{-}(\kappa^1\text{-}\kappa^1)\text{-}(\kappa^0\text{-}\kappa^2)\text{-}\mu_6$ coordination mode (Mode II) and links Co^{II} into a 3D framework in presence of 1,3-bimb ligands, consisting of unreported $[Co_4(\mu_3\text{-}OH)_2]^{6+}$ tetrameric SBUs. With the help of 1,3-bimb ligands, Zn^{II} ions are coordinated by partly deprotonated H_2BPT ligands ($(\kappa^1\text{-}\kappa^0)\text{-}(\kappa^1\text{-}\kappa^0)\text{-}\mu_2$, Mode III), resulting a supramolecular architecture. H_3BPT exhibits two kinds of new coordination modes in **4**: $(\kappa^1\text{-}\kappa^1)\text{-}\mu_2$ coordination mode (Mode IV) for the partly deprotonated one and $(\kappa^0\text{-}\kappa^0)\text{-}(\kappa^1\text{-}\kappa^1)\text{-}(\kappa^1\text{-}\kappa^1)\text{-}\mu_4$ for the completely deprotonated one (Mode V). Co^{II} ions are linked together to form one 2D structure. In **5**, BPT^{3-} exhibit $(\kappa^1\text{-}\kappa^0)\text{-}(\kappa^1\text{-}\kappa^1)\text{-}(\kappa^1\text{-}\kappa^1)\text{-}\mu_5$ coordination mode to link Mn^{II} cations into a 3D framework containing 1D double helix chains. To the best of our knowledge, Mode II, IV, and V have never been documented up to now. As shown in the Scheme 3 and Table 2, other six kinds of coordination modes of H_3BPT (Mode VII-XII) in presence of phenanthroline (phen) and 4,4'-bipyridine (4,4'-bipy) were reported.[19] The results proved that the ancillary ligands have a great effect on the coordination modes of the host polycarboxylate aromatic acid and the final packing structures. The bis(imidazole) bridging linkers have an advantage over other N-donors due to that they can modulate their conformations and coordination modes to satisfy the coordination geometry of metal centers or metal cluster, resulting in interpenetrated and high-dimensional architecture.

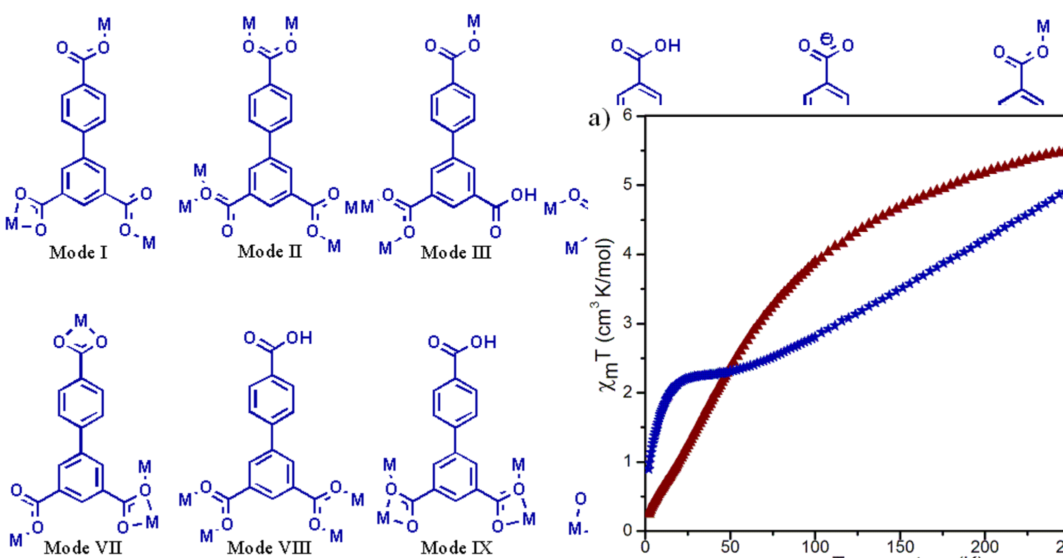

Scheme 3. The coordination modes of H_3BPT in complexes **1**-**5**.

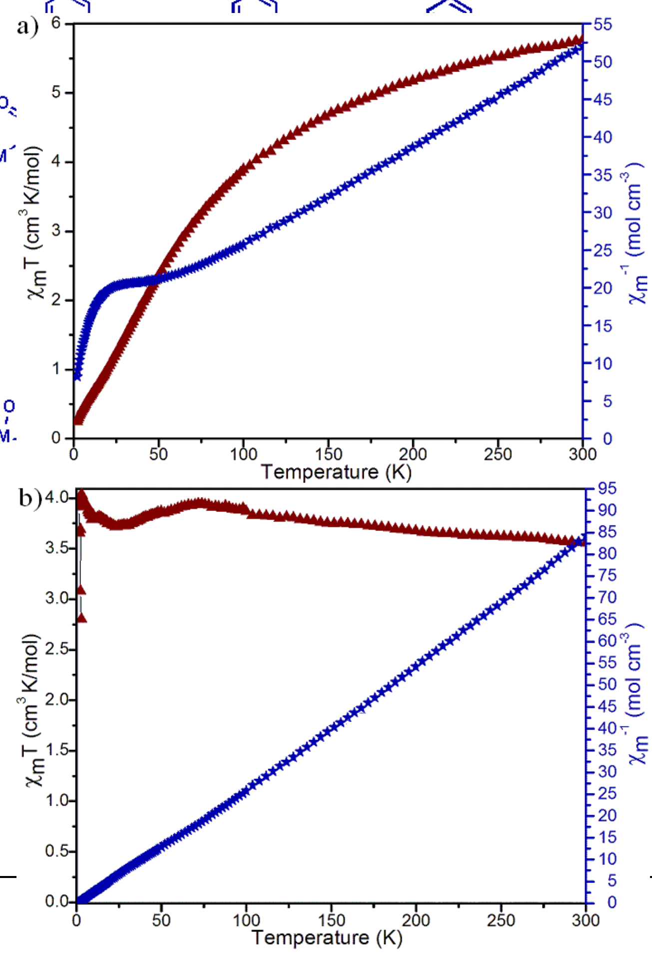

Thermal Analyses. The experiments of thermogravimetric analysis (TGA) were performed on samples of **1**-**5** under N_2 atmosphere with a heating rate of 10 °C min^{-1}, shown in Fig. S7. For **1**, the first weight loss in the temperature range of 80-120°C is consistent with the removal of the coordinated and lattice water molecules (obsd 5.4 %, calcd 5.7 %). The second weight loss of 16.8 % (calcd: 17.2 %) at *ca.* 150°C corresponds to the loss of the guest molecule of 1,4-bib. Then the anhydrous network starts to collapse above 275 °C. For **2**, an initial weight loss of 2.4 % corresponds to the loss of solvent water (calcd: 2.6 %). The second weight loss corresponds to the loss of the organic ligands. For **3**, the first weight loss from 80 to 110 °C is attributed to the loss of lattice water molecules (obsd 2.9 %, calcd 3.0 %). Above 290 °C, it starts to lose its ligands as a result of thermal decomposition. For **4**, the loss of lattice water molecules (obsd 3.1 %, calcd 2.8 %) is observed below 150 °C. The weight loss corresponding to the release of organic ligands is observed above 310 °C. For **5**, the weight loss of water molecules is observed in the range of 95–125 °C (obsd: 1.9 % and calcd: 1.4 %). The decomposition of organic ligands began from 295 °C.

Magnetic Properties. The variable-temperature magnetic susceptibility of **2**, **4**, and **5** were performed in the temperature range of 2-300 K under a field of 1000 Oe. The temperature dependence of $\chi_M T$ and χ_M^{-1} are displayed in Fig. 6 and Fig. 7.

The $\chi_M T$ value for **2** at room temperature is 5.75 cm^3 K mol^{-1} and lower than the theoretical one (7.48 cm^3 K mol^{-1}) for four high-spin Co(II) ions (S = 3/2), which can be attributed to the susceptible contribution from orbital angular momentum at higher temperatures, indicating the overall antiferromagnetic coupling.[20] The $\chi_M T$ values for **4** at room temperature is 3.74 cm^3 K mol^{-1}, slightly lower than the value expected for two isolated

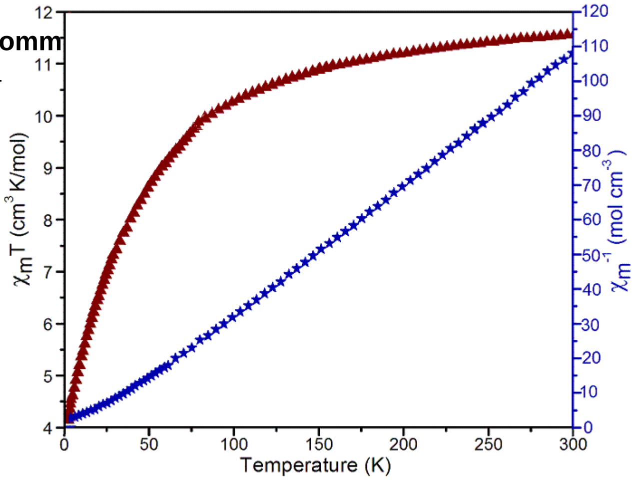

high-spin Co(II) ions (3.75 cm^3 K mol^{-1}). With the temperature decreasing, the $\chi_M T$ value decreases evenly and the value of χ_M increases continuously. The above features all indicate overall antiferromagnetic coupling between Co(II) centers.[21] For **5**, the value fo $\chi_M T$ at room temperature is 11.56 cm^3 K mol^{-1}, lower than the value for five isolated high-spin Mn(II) ions (21.87 cm^3 K mol^{-1}), which can be attributed to the susceptible contribution from orbital angular momentum at higher temperatures, indicating the overall antiferromagnetic coupling.[22]

Figure 6. The temperature dependence of magnetic susceptibility of **2** (a) and **4** (b) under a static field of 1000 Oe.

Figure 7. The temperature dependence of magnetic susceptibility of **5** under a static field of 1000 Oe.

Conclusions

In summary, five coordination polymers were synthesized based on biphenyl-3,4',5-tricarboxylic acid (H_3BPT) and three bis(imidazole) bridging linkers (1,4-bib, 1,3-bimb, and 4,4'-bibp) under hydrothermal conditions. Structural comparison of these networks reveals that the (bis)imidazole bridging ligands have great effect on the coordination modes of H_3BPT, such as Mode II, IV, and V, which have never been documented to date. With the length of the (bis)imidazole ligands increasing, the longer separation of neighboring central ions makes the host aromatic polycarboxylate ligand adopt more "open" coordination modes, and the overall structure a higher degree of interpenetration. The more flexibility of ancillary ligands could make the final structure more twisted and complicated. Moreover, magnetic studies indicate complexes **2**, **4**, and **5** show antiferromagnetic properties.

Acknowledgements

The work was supported by financial support from the Natural Science Foundation of China (Grant Nos. 21101097, 91022034 and 51172127), the Excellent Youth Foundation of Shandong Scientific Committee (Grant JQ201015), and Qilu Normal University is acknowledged.

Notes

The authors declare no competing financial interest.

References

1. (a) G. Férey and C. Serre, *Chem. Soc. Rev*., 2009, **38**, 1380; (b) B. L. Chen, N. W. Ockwig, A. R. Millward, D. S. Contreras and O. M. Yaghi, *Angew. Chem. Int. Ed*., 2005, **44**, 4745; (c) J. Duan, Z. Yang, J. Bai, B. Zheng, Y. Li and S. Li, *Chem. Commun*., 2012, **48**, 3058; (d) J. Duan, M. Higuchi, S. Horike, M. L. Foo, K. P. Rao, Y. Inubushi, T. Fukushima and S. Kitagawa, *Adv. Funct. Mater.*, 2013, **23**, 3525; (e) J. Duan, M. Higuchi, R. Krishna, T. Kiyonaga, Y. Tsutsumi, Y. Sato, Y. Kubota, M. Takata and S. Kitagawa, *Chem. Sci.*, 2014, **5**, 660.
2. (a) M. Kim, J. F. Cahill, H. Fei, K. A. Prather and S. M. Cohen, *J. Am. Chem. Soc*., 2012, **134**, 18082; (b) H. Fei, J. F. Cahill, K. A. Prather and S. M. Cohen, *Inorg. Chem.*, 2013, **52**, 4011; (c) C. X. Chen, Q. K. Liu, J. P. Ma and Y. B. Dong, *J. Mater. Chem.*, 2012, **22**, 9027; (d) Y. Cui, Y. Yue, G. Qian and B. L. Chen, *Chem. Rev.*, 2012, **112**, 1126.
3. (a) D. Sun, S. Yuan, H. Wang, H. F. Lu, S. Y. Feng and D. F. Sun, *Chem. Commun*., 2013, **49**, 6152; (b) B. X. Zhu, Q. L. Zhang, Y. Q. Zhang, Z. Tao, J. K. Clegg, J. R. Reimers, L. F. Lindoy and G. Wei, *Dalton. Trans*., 2009, 4896; (c) X. T. Zhang, L. M. Fan, X. Zhao, D. Sun, D. C. Li and J. M. Dou, *CrystEngComm*, 2012, **14**, 2053.
4. (a) F. Cao, S. Wang, D. Li, S. Zeng, M. Niu, Y. Song and J. Dou *Inorg. Chem.*, 2013, **52**, 10747; (b) X. T. Zhang, D. Sun, B. Li, L. M. Fan, B. Li and P. H. Wei, *Cryst. Growth Des.*, 2012, **12**, 3845; (c) J. B. Lin, W. Xue, B. Y. Wang, J. Tao, W. X. Zhang, J. P. Zhang and X. M. Chen, *Inorg. Chem*., 2012, **51**, 9423.
5. (a) X. Zhang, L. Fan, W. Zhang, Y. Ding, W. Fan and X. Zhao, *Dalton. Trans*., 2013, **42**, 16562; (b) X. J. Liang, X. D. Chen and J. C. Zhao, *Chem. Soc. Rev*., 2014, **43**, 473; (c) H. Fu, Y. G. Li, Y. Liu, W. L. Chen, Q. Wu, J. X. Meng, X. L. Wang, Z. M. Zhang and E. B. Wang, *Cryst. Growth Des.,* 2011, **11**, 458; (d) W. Wang, J. Yang, W. Q. Kan and J. F. Ma, *CrystEngComm.,* 2013, **15**, 5844.
6. (a) P. V. Dau and S. M. Cohen, *Chem. Commun.*, 2013, **49**, 6128; (b) Y. Wang, H. X. Lin, L. Chen, S. Y. Ding, Z. C. Lei, D. Y. Liu, X. Y. Cao, H. J. Liang, Y. B. Jiang and Z. Q. Tian, *Chem. Soc. Rev*., 2014, **43**, 399.
7. (a) J. Duan, B. Zheng, J. Bai, Q. Zhang and Y. Zuo, *Inorg. Chem. Acta*, 2010, **363**, 3172; (b) L. M. Fan, X. T. Zhang, D. C. Li, D. Sun, W. Zhang and J. M. Dou, *CrystEngComm*, 2013, **15**, 349.
8. (a) F. F. B. J. Janssen, L. P. J. Veraart, J. M. M. Smits, R. D. Gelder and A. E. Rowen, *Cryst. Growth Des.*, 2011, **11**, 4313; (b) S. Banerjee, N. N. Adarsh and P. Dastidar, *Cryst. Growth Des.*, 2012, **12**, 6061.
9. (a) J. Li, L. Li, J. Liang, P. Cheng, J. Yu, Y. Xu and R. Xu, *Cryst. Growth Des.*, 2008, **8**, 2318; (b) S. Wang, R. Yun, Y. Peng, Q. Zhang, J. Lu, J. Dou, J. Bai, D. Li and D. Wang, *Cryst. Growth Des.*,

2012, **12**, 79.
10. (a) Q. Yu, Q. Zhang, H. Bian, H. Liang, B. Zhao, S. Yan and D. Liao, *Cryst. Growth Des.*, 2008, **8**, 1140; (b) Y. B. Wang, Y. L. Lei, S. H. Chi and Y. J. Luo, *Dalton Trans.,* 2013, **42**, 1862.
11. (a) W. Hong, H. Lee, T. H. Noh and O. S. Jung, *Dalton Trans.,* 2013, **42**, 11092; (b) C. Zhan, C. Zou, G. Q. Kong and C. D. Wu, *Cryst. Growth Des.*, 2013, **13**, 1429; (c) Q. L. Zhang, P. Hu, Y. Zhao, G. W. Feng, Y. Q. Zhang, B. X. Zhu and Z. Tao, *J. Solid State Chem.,* 2014, **210**, 178.
12. (a) Z. Wu, W. Sun, Y. Chai, W. Zhao, H. Wu, T. Shi and X. Yang, *CrystEngComm*, 2014, **16**, 406; (b) L. Ma, N. Yu, S. Chen and H. Deng, *CrystEngComm*, 2013, **15**, 1352; (c) F. Guo, B. Zhu, M. Liu, X. Zhang, J. Zhang and J. Zhao, 2013, **15**, 6191.
13. (a) P. V. Dau, K. K. Tanabe and S.M. Cohen, *Chem. Commun.*, 2013, **49**, 9370; (b) P. V. Dau, M. Kim and S. M. Cohen, *Chem. Sci.*, 2012, **4**, 601.
14. (a) A. G. Wong-Foy, O. Lebel and A. J. Matzger, *J. Am. Chem. Soc.*, 2007, **129**, 15740; (b) C. S. Lim, J. K. Schnobrich, A. G. Wong-Foy and A. J. Matzger, *Inorg. Chem.*, 2010, **49**, 5271.
15. (a) R. Singh and P. K. Bharadwaj, *Cryst. Growth Des*., 2013, **13**, 3722; (b) X. T. Zhang, L. M. Fan, Z. Sun, W. Zhang, D. C. Li, J. M. Dou J. M. and Han, L. *Cryst. Growth Des*., 2013, **13**, 792; (c) X. T. Zhang, L. M. Fan, W. Zhang, Y. S. Ding, W. L. Fan, L. M. Sun, X. Zhao and H. Lei, *Cryst. Growth Des*., 2013, **13**, 2462; (d) L. Fan, X. Zhang, W. Zhang, Y. Ding, L. Sun, W. Fan and X. Zhao, *CrystEngComm*, 2013, DOI: 10.1039/C3CE42203H.
16. (a) G. M. Sheldrick, *SHELXTL*, version 5.1; Bruker Analytical X-ray Instruments Inc.: Madison, WI, 1998. (b) G. M. Sheldrick, *SHELX-97*, PC Version; University of Gottingen: Gottingen, Germany, 1997.
17. (a) V. A. Blatov, A. P. Shevchenko and V. N. Serezhkin, *J. Appl. Crystallogr.*, 2000, **33**, 1193; (b) The network topology was evaluated by the program “TOPOS-4.0”, see: http://www.topos.ssu.samara.ru. (c) V. A. Blatov, M. O'Keeffe and D. M. Proserpio, *CrystEngComm*, 2010, **12**, 44.
18. (a) A. L. Spek, *J. Appl. Crystallogr.*, 2003, **36**, 7; (b) A. L. Spek, *PLATON, A Multipurpose Crystallographic Tool*, Utrecht University, Utrecht, The Netherlands, 2002.
19. (a) L. Li, J. Luo, S. Wang, Z. Sun, T. Chen and M. Hong, *Cryst. Growth Des.*, 2011, **11**, 3744; (b) Y. Lu, W. Zhao, Y. Liu, B. Liu, X. Feng, J. Tan and X. Yang, *J. Solid State Chem.*, 2012, **144**, 192; (c) C. C. Ji, J. Li, Y. Z. Li, Z. J. Guo and H. G. Zheng, *CrystEngComm.,* 2011, **13**, 459.
20. (a) M. Ahmad, M. K. Sharma, R. Das, P. Poddar and P. K. Bharadwaj, *Cryst. Growth Des.*, 2012, **12**, 1571; (b) Q. Chen, W. Xue, J. B. Lin, R. B. Lin, M. H. Zeng and X. M. Chen, *Dalton. Trans*., 2012, **41**, 4199.
21. (a) H. Zhou, G. X. Liu, X. F. Wang and Y. Wang, *CrystEngComm.*, 2013, **15**, 1377; (b) S. Y. Song, X. Z. Song, S. N. Zhao, C. Qin, S. Q. Su, M. Zhu, Z. M. Hao and H. J. Zhang, *Dalton. Trans*., 2012, **41**, 10412; (c) L. F. Ma, X. Q. Li, B. Liu, L. Y. Wang and H. W. Hou, *CrystEngComm.*, 2011, **13**, 4973.
22. Y. Ma, K. Wang, E. Q. Gao and Y. Song, *Dalton. Trans*., 2010, **39**, 7714.

CrystEngComm

For Table of Contents Use Only

Table of Contents Graphic and Synopsis

Syntheses, Structures, and Magnetic Properties of Five Coordination Polymers Constructed From Biphenyl-3,4',5-Tricarboxylic Acid And (Bis)imidazole Linkers

Xiutang Zhang, Liming Fan, Wei Zhang, Weiliu Fan, Liming Sun, Xian Zhao

Five multi-dimensional coordination polymers (CPs), $\{[Ni_{1.5}(BPT)(1,4\text{-bib})_2(H_2O)]\cdot(1,4\text{-bib})_{0.5}\cdot 2H_2O\}_n$ (**1**), $\{[Co_2(BPT)(1,3\text{-bimb})(\mu_3\text{-}OH)]\cdot H_2O\}_n$ (**2**), $\{[Zn(HBPT)(1,3\text{-bimb})]\cdot H_2O\}_n$ (**3**), $\{[Co_2(BPT)(H_2BPT)(4,4'\text{-bibp})_2]\cdot 2H_2O\}_n$ (**4**), and $[Mn_{2.5}(BPT)(4,4'\text{-bibp})_{2.5}(SO_4)(H_2O)]_n$ (**5**) (H_3BPT = biphenyl-3,4',5-tricarboxylic acid, 1,4-bib = 1,4-bis(1H-imidazol-4-yl)benzene, 1,3-bimb = 1,3-bis(imidazol-1-ylmethyl)benzene, 4,4'-bibp = 4,4'-bis(imidazol-1-yl)biphenyl), were synthesized under hydrothermal conditions. Complex **1** exhibits an unprecedented 2D+2D→3D parallel entangled networks consisting of trilayer (3,4,6)-connected $(4^4.5^4.6^6.8)(5.6^4.8)_2(5^2.6^2)$ sheets. Complex **2** dispalys a 3D (3,10)-connected **3,10T9** net based on tetranuclear $\{Co_4(\mu_3\text{-}OH)_2\}$ clusters with the Schläfli symbol of $(4^{18}.6^{24}.8^3)(4^3)_2$. Complex **3** shows an interesting 1D tube-like chain including $Zn_2(1,3\text{-bimb})_2$ loops. Complex **4** affords a 2D $(4^4.6^2)$-**sql** net constructed from $\{Co_2\}$ dinuclear units. Complex **5** dispalys a 3D 6-connected $(4^{12}.6^3)$-**pcu** net consisting of α-po primitive $\{Mn_5(SO_4)_2\}$ cube. Magnetic studies indicate complexes **2**, **4** and **5** show antiferromagnetic properties.